Ore Geology Reviews 49 (2012) 85–95

Contents lists available at SciVerse ScienceDirect

Ore Geology Reviews

journal homepage: www.elsevier.com/locate/oregeorev

Geology and fluid evolution of the Wangfeng orogenic-type gold deposit, Western Tian Shan, China

Li Zhang [a], Huayong Chen [a,b,*], Yanjing Chen [c], Yajing Qin [a,d], Chunfa Liu [a,d], Yi Zheng [a,d], Nicholas H. Jansen [b]

[a] Key Laboratory of Mineralogy and Metallogeny, Guangzhou Institute of Geochemistry, Chinese Academy of Sciences, Guangzhou 510640, China
[b] ARC Centre of Excellence in Ore Deposit Research (CODES), University of Tasmania, TAS 7001, Australia
[c] Key Laboratory of Crust and Orogen Evolution, Peking University, Beijing 100871, China
[d] Graduate University of Chinese Academy of Sciences, Beijing, China

ARTICLE INFO

Article history:
Received 23 January 2012
Received in revised form 4 September 2012
Accepted 6 September 2012
Available online 13 September 2012

Keywords:
Wangfeng gold deposit
Fluid inclusion
Orogenic gold deposit
Western Tian Shan

ABSTRACT

The Wangfeng gold deposit is located in Western Tian Shan and the central section of the Central Asian Orogenic Belt (CAOB). The deposit is mainly hosted in Precambrian metamorphic rocks and Caledonian granites and is structurally controlled by the Shenglidaban ductile shear zone. The gold orebodies consist of gold-bearing quartz veins and altered mylonite. The mineralization can be divided into three stages: quartz–pyrite veins in the early stage, sulfide–quartz veins in the middle stage, and quartz–carbonate veins or veinlets in the late stage. Ore minerals and native gold mainly formed in the middle stage. Four types of fluid inclusions were identified based on petrography and laser Raman spectroscopy: CO_2–H_2O inclusions (C-type), pure CO_2 inclusions (PC-type), NaCl–H_2O inclusions (W-type), and daughter mineral-bearing inclusions (S-type). The early-stage quartz contains only primary CO_2–H_2O fluid inclusions with salinities of 1.62 to 8.03 wt.% NaCl equivalent, bulk densities of 0.73 to 0.89 g/cm^3, and homogenization temperatures of 256 °C–390 °C. Vapor bubbles are composed of CO_2. The middle-stage quartz contains all four types of fluid inclusions, of which the CO_2–H_2O and NaCl–H_2O types yield homogenization temperatures of 210 °C–340 °C and 230 °C–300 °C, respectively. The CO_2–H_2O fluid inclusions have salinities of 0.83 to 9.59 wt.% NaCl equivalent and bulk densities of 0.77 to 0.95 g/cm^3, with vapor bubbles composed of CO_2, CH_4, and N_2. Fluid inclusions in the late-stage quartz are NaCl–H_2O solution with low salinities (0.35–3.87 wt.% NaCl equivalent) and low homogenization temperatures (122 °C–214 °C). The coexistence of inclusions of these four types in middle-stage quartz suggests that fluid boiling occurred in the middle-stage mineralization. Trapping pressures estimated from CO_2–H_2O inclusions are 110–300 MPa and 90–250 MPa for the early and middle stages, respectively, suggesting that gold mineralization mainly occurred at depths of about 10 km. In general, the Wangfeng gold deposit originated from a metamorphic fluid system characterized by low salinity, low density, and enrichment of CO_2. Depressurized fluid boiling caused gold precipitation. Given the regional geology, ore geology, fluid-inclusion features, and ore-forming age, the Wangfeng gold deposit can be classified as a hypozonal orogenic gold deposit.

© 2012 Elsevier B.V. All rights reserved.

1. Introduction

Orogenic gold deposits are the main source of gold in the world and their geological and geochemical characteristics have been well summarized (e.g., Chen, 2006, 2010; Chen et al., 2007; Goldfarb et al., 2001; Groves and Beirlein, 2007; Groves et al., 1998; Kerrich et al., 2000) as follows: (1) They are usually associated with metamorphic terranes at convergent margins, including accretionary and collisional orogens; (2) the locations and occurrences of the orebodies are controlled by shear zones or faults; (3) orogenic-type mineralization depth ranges are from 5 to 20 km, and possibly connected with epizonogenic mineralization at shallower levels; (4) mineralization is coeval with orogenies, particularly, at the tectonic transition phase from compression to extension, or in transcompressional settings; and (5) the ore fluids are generally carbonic or CO_2-rich with variable CH_4, generated from metamorphic devolatilization.

The Central Asian Orogenic Belt (CAOB) is commonly accepted as an accretionary orogen that experienced episodic oceanic plate subduction and continental growth in the Neoproterozoic to the Permian, with final oceanic closure followed by intercontinental collision during the Late Carboniferous to the Early Triassic (Chen, 2000; Chen and Jahn, 2004; Sengor and Natal'in, 1996; Xiao et al., 2008, 2009, and reference therein). The CAOB is an important metalliferous province hosting numerous mineral systems (e.g., Cu, Au, Pb, and Zn) formed during the Neoproterozoic to the Triassic, but with the majority formed in the Late Paleozoic.

The Western Chinese Tian Shan is an important part of the CAOB as it is favorable for orogenic-type mineralization when considering

* Corresponding author at: Key Laboratory of Mineralogy and Metallogeny, Guangzhou Institute of Geochemistry, Chinese Academy of Sciences, Guangzhou 510640, China.
E-mail address: huayongchen@gig.ac.cn (H. Chen).

0169-1368/$ – see front matter © 2012 Elsevier B.V. All rights reserved.
http://dx.doi.org/10.1016/j.oregeorev.2012.09.002

metallogenic models for either subduction-related accretionary orogeny (Goldfarb et al., 1991, 2001) or continental collisional orogeny (Chen and Fu, 1992; Chen et al., 2004, 2012a; Pirajno, 2009). However, so far only the Tianger gold belt has been reported to be orogenic-type in this area (Chen et al., 2000; Zhu et al., 2007), which makes the Tianger gold belt (including the Wangfeng gold deposit) a useful window for providing insight into orogenic-type mineralization in the Western Chinese Tian Shan.

This paper presents a detailed fluid-inclusion study of the Wangfeng gold deposit, clarifies the nature and evolution of the ore-forming fluid system, and probes the ore genesis of the deposit.

2. Regional geology

The CAOB is an orogenic collage, comprising ophiolite suites, magmatic arcs, Precambrian massifs, and accretionary terranes resulting from the collision between the Siberia and Tarim–Sino-Korean plates along the Solonker suture that diachronously closed during the Carboniferous to Early Triassic (Chen et al., 2007, 2009, 2012a; Sengor and Natal'in, 1996; Xiao et al., 2009). Despite the diachronous oceanic closure, the CAOB is generally accepted as a Late Paleozoic (320–250 Ma) or Hercynian subduction-related accretionary orogenic belt (Xiao et al., 2009).

North Xinjiang, which is a key part of the CAOB, refers to the area north of the Tarim Basin in Central Asia and has a complex tectonic framework (Fig. 1; Chen, 2000; Xiao et al., 2008). The Chinese Altay Shan is an accretionary complex on the southern margin of the Siberia continental plate, with the Erqis (also known as Irtysh) tectonic suture as its southern boundary. The area from the Erqis suture southward to the Southern Tian Shan (or Kumishi) accretionary complex, including Eastern and Western Junggar orogenic belts, Junggar Basin, Turpan Basin, and Tian Shan, constitutes a wide Tian Shan–Junggar accretionary belt that can be regarded as a part of the Kazakhstan plate (Fig. 1).

The Western Chinese Tian Shan is the area between Tarim and Junggar basins and is generally divided into three tectonic units. The tectonic units, from north to south, are the Northern Tian Shan (NTS) accretionary belt, the Central Tian Shan (CTS)–Ili block, and the Southern Tian Shan (STS) accretionary belt, with the Bingdaban and Kumishi Faults as their boundaries (Fig. 1). The CTS–Ili block is characterized by the presence of a Precambrian metamorphic basement intruded by numerous granitic rocks with ages from Permian to occasionally Neoproterozoic (Chen and Chang, 2000) and locally covered by Late Paleozoic volcanic rocks such as the Dahalajunshan Formation.

The NTS accretionary belt is roughly divided into two parts by the E–W-trending Kangur Fault system (Fig. 1; the Hongwuyueqiao Fault in Fig. 2). The Bayinggou–Kangur ophiolite slices, which have been interpreted as records of the Carboniferous intra-arc rifting basin, occur along the Kangur Fault. The accretionary belt between the Bindaban and Kangur Faults was mainly formed in the Early Paleozoic, and in the study area they are represented by the Kekenaike Group, which is composed of the greenschist-facies metamorphosed Ordovician volcanic–sedimentary sequences including spilite–keratophyre, greywacke, and clastic rocks. This accretionary complex is locally, unconformably overlain by the Late Paleozoic volcanic–sedimentary sequences, bounded with the Hongwuyueqiao Fault (Fig. 2). The area between the Kangur and Kalameili Faults comprises various Late Paleozoic accretionary complexes and occasionally Early Paleozoic terranes. In the studied area it includes mainly the Carboniferous Qiergusitao Group composed of thick-bedded clastic rocks, andesitic lava, and breccia intercalated with limestone, chert and shale.

The Bingdaban Fault strikes more than 50 km in the studied area, with a width of 3–4 km. The Shenglidaban ductile shear zone, paralleling to the Bingdaban Fault but narrowing to the south, occurs in the Precambrian granite–migmatite–gneiss complex and controls the location of gold deposits of the Tianger gold belt, such as the Saridala, Wangfeng, and Asuwo gold deposits from west to east (Fig. 2).

The Paleozoic granitic intrusions are widely developed in the Tianger gold belt. The Early Paleozoic (Caledonian) intrusions are intensively deformed and locally altered, whereas the Late Paleozoic–Triassic (Hercynian) granites (e.g., Wulasitai granite in the south of Wangfeng) are not metamorphosed. Two episodic dikes are also

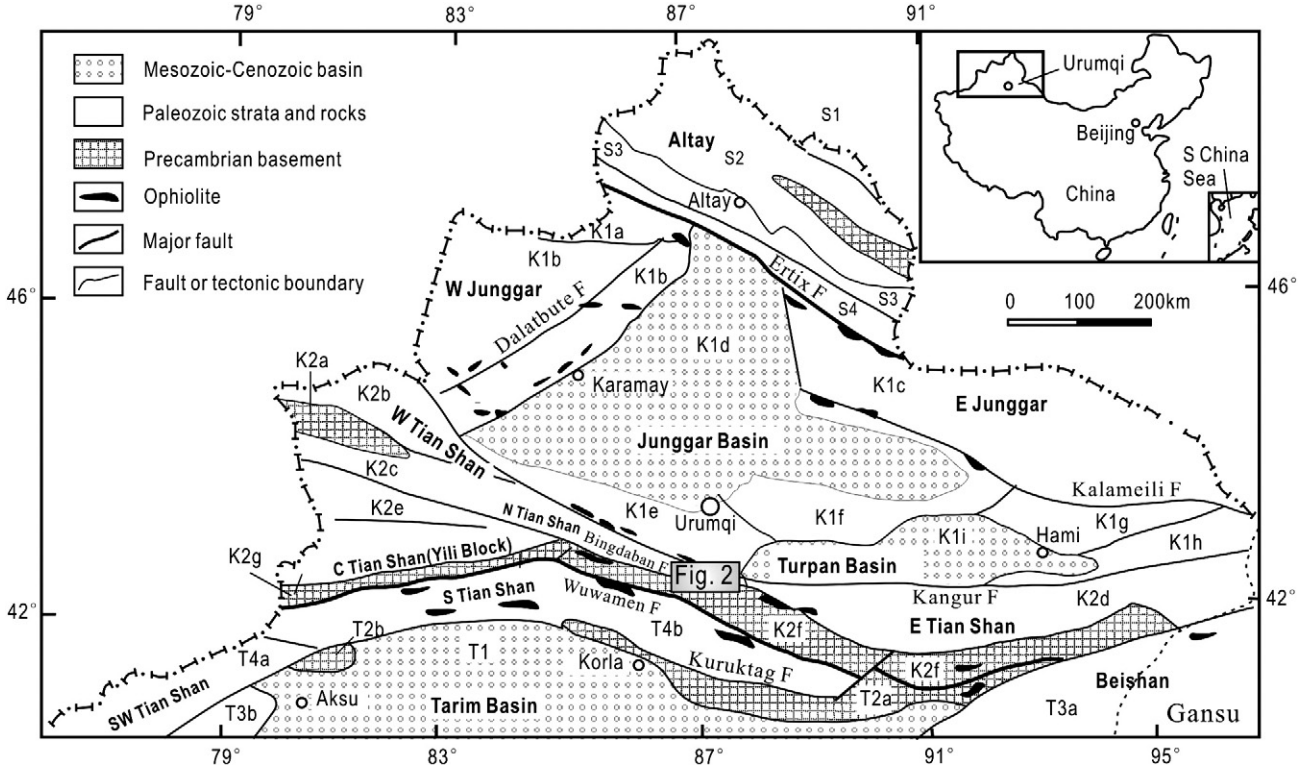

Fig 1. Sketch map showing the tectonic framework of north Xinjiang (simplified after Chen et al., 2012a).

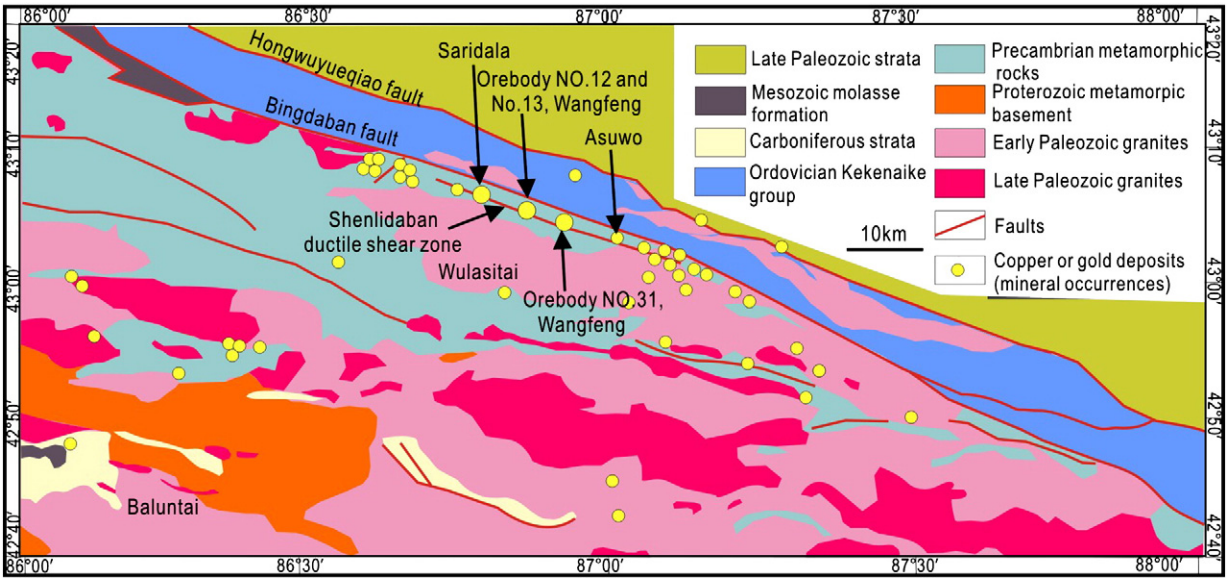

Fig. 2. Simplified regional geological map of the Wangfeng gold deposit (modified after Chen and Chang, 2000).

recognized in the Tianger gold belt. The early lamprophyre dikes were fractured and hydrothermally altered, trending roughly parallel to the Bingdaban Fault and yielding a zircon SHRIMP U–Pb age of 418.1 ± 7.5 Ma. The younger diabase dikes show no remarkable deformation or alteration, and occasionally cross-cut the gold orebodies in the Tianger gold belt.

3. Deposit geology

The Wangfeng gold deposit is situated in the eastern segment of the Western Chinese Tian Shan and tectonically located at the northern margin of the Central Tian Shan, approximately 110 km southwest of the Urumqi City, Xinjiang Province, China (Figs. 1 and 2;

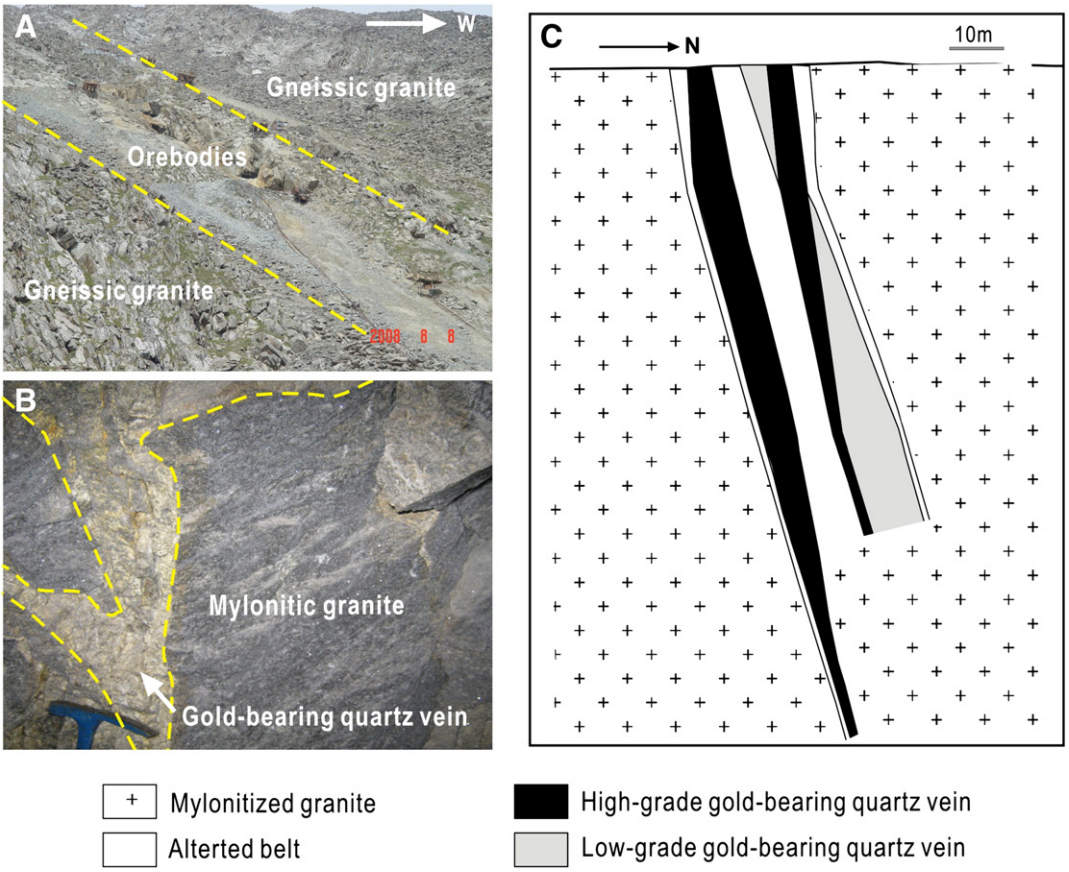

Fig. 3. A. Photograph showing an outcrop of the Wangfeng gold deposit. B. Photograph showing gold-bearing quartz vein and wall rocks. C. Geological profile of No. 5 prospecting line of No. 12 orebody in the Wangfeng gold deposit (after Geological Team 1 of the Xinjiang Bureau of Geology and Mineral Resources, 2005).

Chen et al., 1998; Wang et al., 1994, 1995; Wu and Chen, 1999). The Wangfeng gold deposit comprises 13 identified gold-bearing veins, which are restricted to the W–NW-trending Shenglidaban ductile shear zone. The lens-shaped orebodies generally strike N0° to 20° and dip 65° to 85°, with lengths of 100 to 3000 m and thicknesses of 1 to 7 m. The largest orebody is the No. 12 quartz lode, which is lenticular, with a length of 300 to 960 m and a thickness of 1.8 to 3.8 m. The Au grade in the No. 12 orebody ranges from 1.42 to 8.59 g/t, with an average of 4.89 g/t (Chen and Chang, 2000). Orebodies are hosted in the Precambrian metamorphic rocks and Caledonian granitic rocks which were strongly deformed and mylonitized (Fig. 3). There is no intrusions outcrop in the deposit area. The massive Wulasitai granite is located >1 km in the south of major orebodies (Fig. 2).

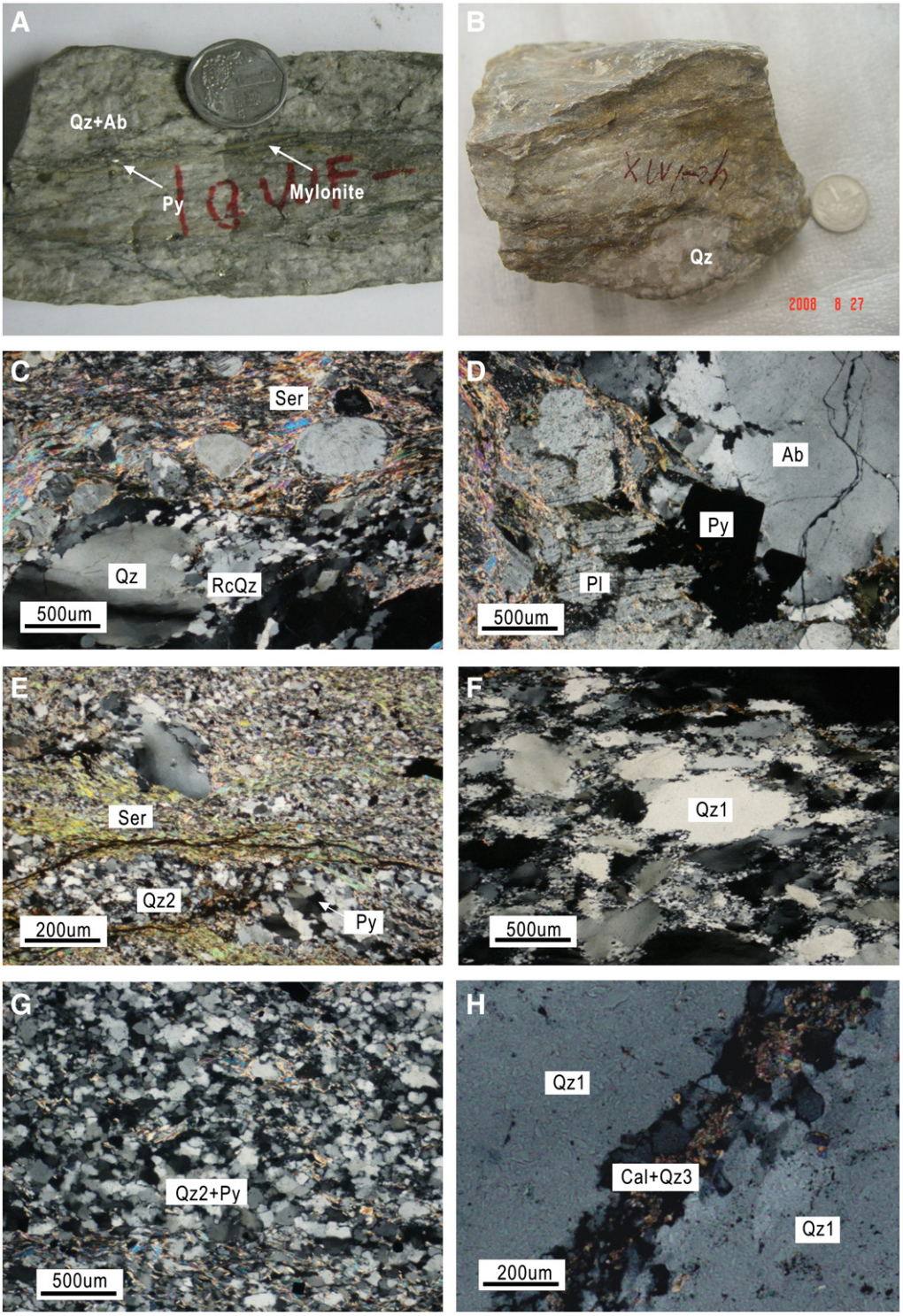

Fig. 4. Photographs showing ore geology of the Wangfeng gold deposit. A. An altered-rock mineralization style. B. A quartz-vein mineralization style. C. A euhedral quartz crystal with fine recrystallized quartz (RcQz). D. Albite with plagioclase replaced by pyrite. E. Alteration assemblage of silicification, sericitization, and pyritization. F. Early-stage euhedral quartz crystals (Qz1) with undulose extinction and pronounced subgrain formation. G. Middle-stage fine-grained quartz (Qz2) associated with sulfides and sericite. H. Late-stage euhedral quartz (Qz3) associated with calcite in a vein cutting early-stage quartz. Qz: quartz, Ab: albite, Py: pyrite, Ser: sericite, Cal: calcite, Pl: plagioclase.

There are two main styles of mineralization in the deposit: (1) mineralization in the altered host rocks surrounding the auriferous quartz veins (Fig. 4A), consisting of disseminated pyrite within the granites, and (2) a quartz-vein (Fig. 4B), in which gold is within quartz veins, principally associated with pyrite.

The major ore minerals include native gold and pyrite. Other subordinate species are pyrrhotite, chalcopyrite, galena, magnetite, and sphalerite. Secondary ore minerals are mainly marcasite and limonite. The main gangue minerals consist of quartz, feldspars and sericite, with minor amounts of chlorite, calcite, titanite, and rutile. Native gold grains occur mainly in tiny fissures of pyrite and quartz or as inclusions in pyrite crystals and gangue minerals (Chen and Chang, 2000).

Hydrothermal alteration including silicification, pyritization, sericitization, albitization, chloritization, and carbonatization is well developed around the orebodies and shear zones. Silicification, pyritization, and sericitization are spatially associated with the gold mineralization (Fig. 4C and E). Pyrite is widely distributed, occurring as veinlets or disseminations along mylonitic foliation. Sericite is intensive in the deformed zone and commonly replaces plagioclase (Fig. 4D).

Based mainly on mineralogical assemblages and alteration processes (Fig. 5), mineralization can be divided into early, middle, and late stages. The early stage is characterized by the assemblage of quartz + pyrite. Quartz (Qz1) in this stage is whitish or milky and euhedral, characterized by undulose extinction and pronounced subgrain formation which indicate intracrystalline deformation (Fig. 4F). The middle stage, characterized by sulfides–quartz veins, represents the main gold-mineralizing event. Quartz (Qz2) in this stage is locally smoky-gray and fine-grained, characterized by some veinlets of pyrite, chalcopyrite and pyrrhotite. Silicification and sericitization are the most conspicuous alteration in this stage (Fig. 4G). The late stage is characterized by quartz + carbonate veins (Qz3), commonly occurring as veinlets cross-cutting the earlier formed quartz (Fig. 4H).

4. Fluid inclusions

4.1. Samples and analytical methods

Doubly polished thin sections (about 0.20 mm thick) were made from 17 quartz samples associated with different stages. Fluid inclusions were carefully observed to identify their genetic and composition types, vapor–liquid ratios, and spatial clustering (Fig. 6). Some typical samples were selected for microthermometric measurements and laser Raman spectroscopy analyses.

Microthermometric measurements were performed using a Linkam TH600 heating–freezing stage which is attached to a Leitz Ortholux transmitted light microscope connected to a television camera and screen at the Guangzhou Institute of Geochemistry, Chinese Academy of Sciences. The stage was calibrated using synthetic fluid inclusions. The estimated accuracy was ±0.1 °C at temperatures below 30 °C and ±1 °C at temperatures above 30 °C. The warming rate was maintained from 0.2 °C to 5 °C min^{-1}, and the heating rate was reduced to 0.2 °C min^{-1} when close to phase-change conditions. Freezing experiments were performed first on all sections to avoid the decrepitation of inclusions.

Final melting temperatures of ice ($T_{m\text{-}ice}$) and clathrate ($T_{m\text{-}clath}$) were measured to calculate salinities of NaCl–H_2O (Bodnar, 1993) and CO_2–H_2O (Collins, 1979) fluid systems, respectively. The melting temperature of CO_2 ($T_{m\text{-}CO_2}$) was measured to evaluate the purity of CO_2 phase. The homogenization temperatures of the CO_2 ($T_{h\text{-}CO_2}$) were used to determine the density of the CO_2, and the total homogenization temperatures ($T_{h\text{-}hot}$) were also measured. The microthermometric data from all types of fluid inclusions are listed in Table 1 and graphically presented in Fig. 7. Calculations of mole fractions of compositions, density of carbonic liquid and bulk fluid, and bulk molar volume of fluid inclusions were performed using the Flincor program of Brown (1989).

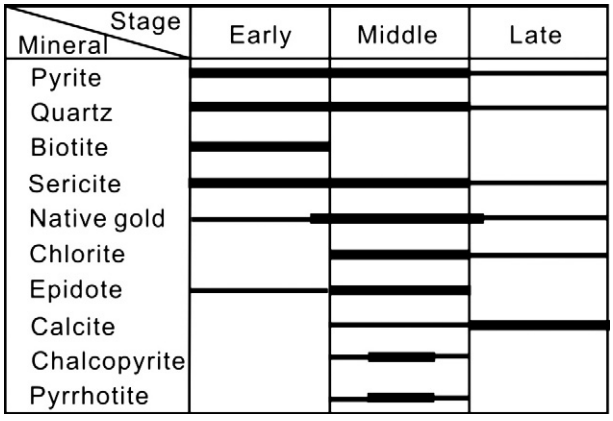

Fig. 5. Paragenetic sequence of the Wangfeng gold deposit (modified after Chen and Chang, 2000).

4.2. Types of fluid inclusions

In this study, four compositional types of fluid inclusions were identified, i.e., CO_2–H_2O (C-type), pure CO_2 (PC-type), aqueous (W-type), and daughter-mineral-bearing (S-type) fluid inclusions, on the basis of their relative phases present at room temperature and phase changes during freezing runs. Inclusions of these four types exist in randomly distributed clusters or occur along three-dimensional arrays and fractures in quartz (Fig. 6).

(1) *C type* inclusions are CO_2–H_2O fluid inclusions, composed of H_2O and CO_2 phases (Fig. 6A), with the CO_2 phase accounting for 15%–85% of the volume. They are the most predominant type of fluid inclusion observed in the early- and middle-stage quartz of the Wangfeng gold deposit. These inclusions exhibit a variety of polygonal forms and range in size from 5 to 20 μm. They are commonly two-phase (liquid CO_2 + liquid H_2O) inclusions at room temperature, but occasionally three-phase inclusions are observed (vapor CO_2 + liquid CO_2 + liquid H_2O). Vapor CO_2 can be also observed in two-phase fluid inclusions through cooling down to 10 °C or below. Most CO_2–H_2O fluid inclusions occur as isolated singles or in clusters of randomly aligned inclusions and they are considered as primary inclusions in this study.

(2) *PC type* inclusions are pure CO_2 or carbonic fluid inclusions. PC-type fluid inclusions show generally oval to subrounded shapes with size varying between 5 and 15 μm. They appear as monophase (liquid CO_2) or two-phase (liquid CO_2 + vapor CO_2) inclusions at room temperature (Fig. 6B). The two-phase inclusions mostly have more liquid than vapor by volume. In some cases, these inclusions display thick dark boundaries, suggesting the presence of a thin H_2O film rimming their inner walls. Carbonic fluid inclusions are found in middle-stage quartz and are interpreted as primary inclusions because they are commonly isolated singles.

(3) *W-type*: These aqueous (H_2O–NaCl) fluid inclusions usually appear as two-phase (liquid water and vapor water) fluid inclusions at room temperature (Fig. 6D), with vapor volume accounting for 5%–15% of the total fluid inclusions. Morphologically, they show variations from negative-crystal shapes to oval, tubular, or irregular forms, and they vary in size from 5 to 15 μm. Trace content of CO_2 can still be identified in the vapor bubbles by laser Raman spectroscopy, although no visible CO_2 phase appears during heating or cooling runs. The primary W-type fluid inclusions occur as isolated singles in middle-stage quartz and the secondary W-type fluid inclusions can be observed as intergranular arrays or trails in early- and middle-stage quartz (Fig. 6D).

(4) *S-type* inclusions are daughter-mineral-bearing or multiphase fluid inclusions. They are rare and usually consist of aqueous liquid, a

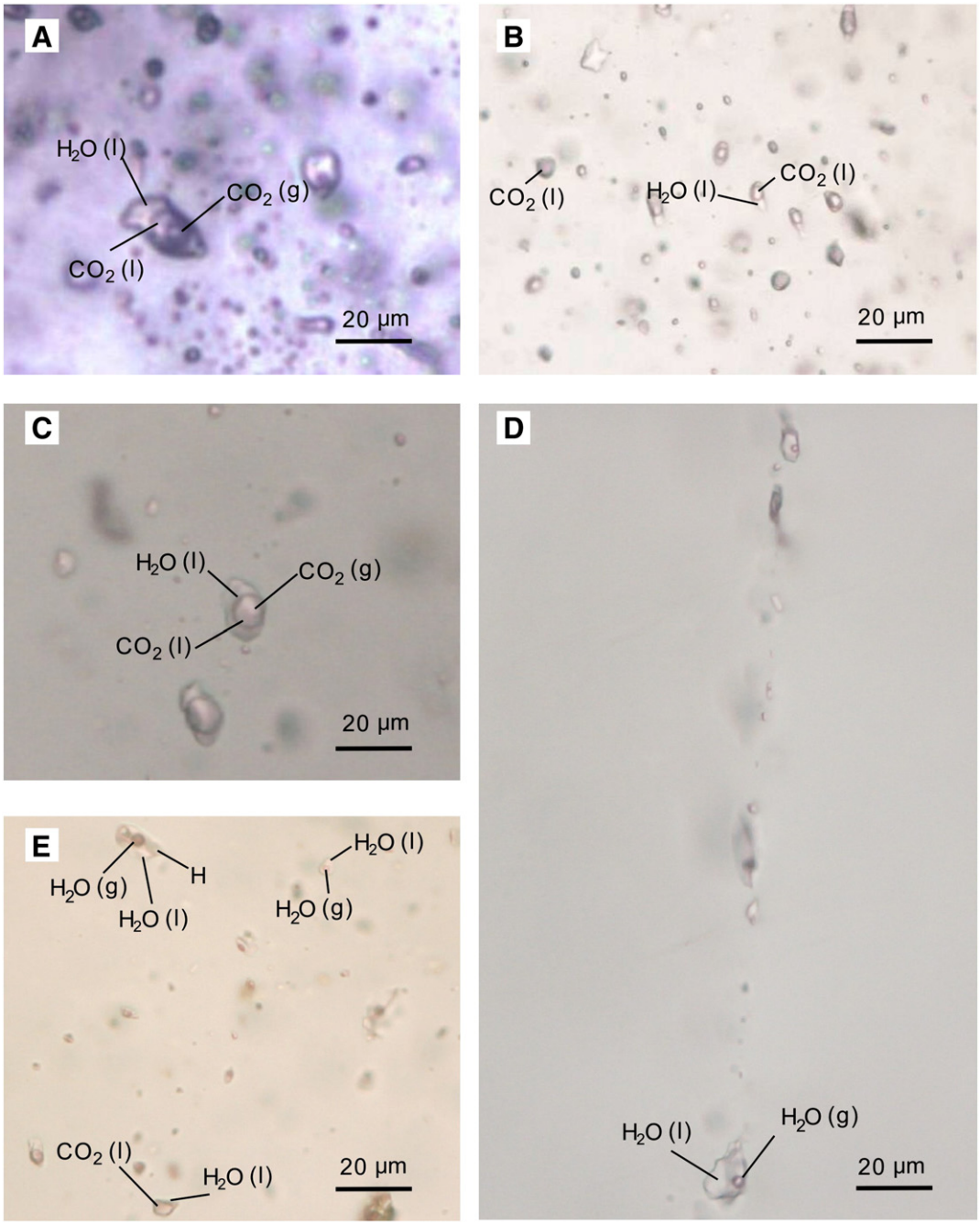

Fig. 6. Microphotographs of typical fluid inclusions in the Wangfeng gold deposit. A. C-type fluid inclusions in early-stage quartz. B. Coexistence of PC-type and C-type fluid inclusions in middle-stage quartz. C. C-type fluid inclusions in the middle stage. D. Secondary W-type fluid inclusions in early-stage quartz. E. Coexistence of C-type, W-type, and S-type fluid inclusions in middle-stage quartz.

vapor bubble, and a halite crystal at room temperature (Fig. 6E). They are irregular to round in shape and 5–8 μm in size. Most of these inclusions probably have a primary origin, as demonstrated by their isolated individuals occurring with other types of fluid inclusions (Fig. 6E).

4.3. Microthermometry

4.3.1. Early stage

Fluid inclusions in the early-stage quartz are dominantly C-type. The melting temperatures of solid CO_2 ($T_{m\text{-}CO_2}$) range from −56.9 °C to −58.3 °C, with a mode at −57.3 °C, slightly below the triple point of pure CO_2 (−56.6 °C). The melting temperatures of clathrates ($T_{m\text{-}clath}$) were observed between 5.6 °C and 9.2 °C, indicating that the salinities are between 1.62 and 8.03 wt.% NaCl equivalent. The carbonic phase ($T_{h\text{-}CO_2}$) was partially homogenized to liquid at temperatures ranging from 2 °C to 31.6 °C. Total homogenization ($T_{h\text{-}hot}$) of the carbonic and aqueous phases (L+V to L, few L+V to V) is observed at temperatures ranging between 256 °C and 390 °C; however, many inclusions with greater vapor/liquid ratios decrepitated prior to final homogenization at about 300 °C. The calculated CO_2 densities range from 0.56 to 0.87 g/cm^3 and bulk densities from 0.73 to 0.89 g/cm^3. Raman analysis shows that the volatile component of these fluid inclusions is dominated by CO_2 and H_2O (Fig. 8A).

4.3.2. Middle stage

The middle-stage quartz contains all types of fluid inclusions identified in the Wangfeng gold deposit (Table 1), among which C-type fluid inclusions are the most abundant. $T_{m\text{-}CO_2}$ ranged from −58.2 °C

Table 1
Microthermometric data of fluid inclusions in the Wangfeng gold deposit.

Stage	Type	Number	$T_{m\text{-}CO_2}$ (°C)	$T_{m\text{-}clath}$ (°C)	$T_{h\text{-}CO_2}$ (°C)	$T_{m\text{-}ice}$ (°C)	$T_{h\text{-}tot}$ (°C)	Salinity (wt.% NaCl equiv.)	CO_2 density (g/cm^3)	Bulk density (g/cm^3)
Early stage	C	30	−56.9 to −58.3	5.6–9.2	2–31.6		260–390	1.62–8.03	0.56–0.87	0.73–0.89
	C	52	−62 to −58.2	4.5–9.6	4.0–22.6		210–340	0.83–9.59	0.71–0.9	0.77–0.95
Middle stage	PC	17	−63.4 to −57.7		−2.8–28.4				0.76–0.94	
	W	17				−5.0 to −2.1	230–300	3.55–7.86		
Late stage	W	12				−0.3 to −2.3	122–214	0.35–3.87		

$T_{m\text{-}CO_2}$ = final melting temperature of solid CO_2.
$T_{m\text{-}clath}$ = final melting temperature of the clathrate phase.
$T_{h\text{-}CO_2}$ = temperature of CO_2 (L+V) to CO_2 (L).
$T_{m\text{-}ice}$ = final melting temperature of water ice.
$T_{h\text{-}tot}$ = temperature of total homogenization of the inclusions.
wt.% NaCl equiv. = weight percent NaCl equivalent.

to −62 °C and is generally lower than that obtained for C-type inclusions in the early-stage quartz and lower than the pure CO_2 melting point (−56.6 °C), indicating the presence of other gasses such as CH_4 and N_2 (Roedder, 1984). Melting of the CO_2 clathrate ($T_{m\text{-}clath}$) in the presence of CO_2 liquid occurs between 4.5 °C and 9.6 °C, giving corresponding fluid salinities of 0.83 to 9.59 wt.% NaCl equivalent. CO_2 generally homogenized to the liquid phase and $T_{h\text{-}CO_2}$ range from 4 °C to 22.6 °C. The densities of the CO_2 phase are calculated to be between 0.71 and 0.9 g/cm^3 and calculated bulk densities range from 0.77 to 0.95 g/cm^3. Most C-type fluid inclusions homogenized in the range of 210 °C to 340 °C, but some inclusions decrepitate at temperatures from 200 °C to 270 °C prior to total homogenization due to high inner pressure.

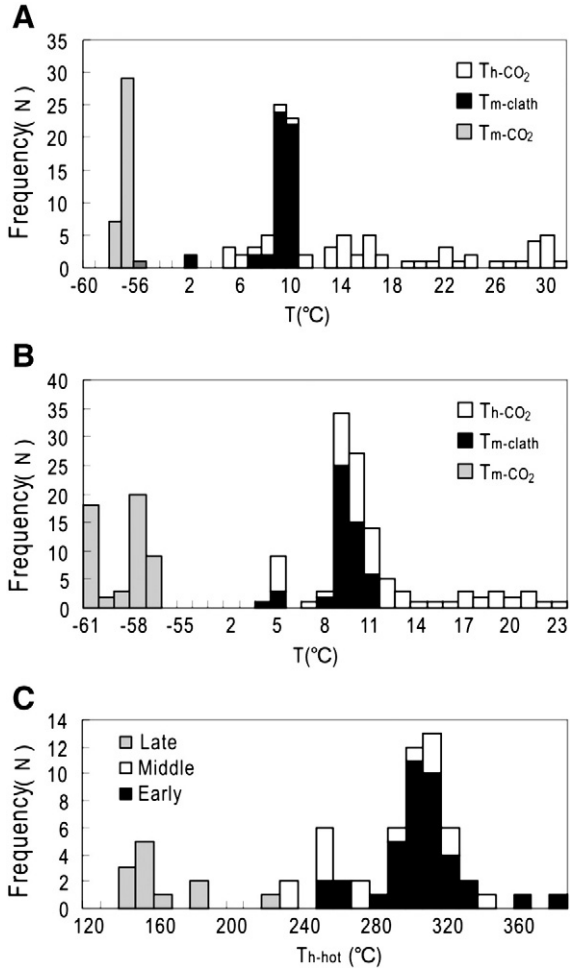

Fig. 7. Histograms of thermometric measurements of fluid inclusions in quartz. A. Microthermometric data of CO_2 and clathrates in fluid inclusions in early-stage quartz. B. Microthermometric data of CO_2 and clathrates in fluid inclusions in middle-stage quartz. C. Histograms of homogenization temperature of fluid inclusion in quartz. $T_{m\text{-}CO_2}$: final melting temperature of solid CO_2; $T_{m\text{-}clath}$: final melting temperature of the clathrate phase; $T_{h\text{-}CO_2}$: homogenization temperature of CO_2 (L+V) to CO_2 (L); $T_{h\text{-}hot}$: temperature of total homogenization of the inclusions.

The PC-type fluid inclusions are generally oval or subrounded and 5 to 15 μm in size. During cooling, PC-type fluid inclusions exhibited two phases and freeze to solid CO_2 + vapor CO_2 below −100 °C. Final melting to liquid was observed during heating, with $T_{m\text{-}CO_2}$ ranging from −63.4 °C to −57.7 °C. Partial homogenization ($T_{h\text{-}CO_2}$) of CO_2 (L+V to L) occurs between −2.8 °C and 28.4 °C, corresponding to densities of 0.76 to 0.94 g/cm^3.

Primary W-type inclusions were only rarely observed in middle-stage quartz. They are usually found in the vicinity of PC- and C-type fluid inclusions, with $T_{m\text{-}ice}$ of −2.1 °C to −5.0 °C. Homogenization occurred to the liquid phase between 230 °C and 300 °C. The estimated salinities range from 3.55 to 7.86 wt.% NaCl equivalent.

S-type fluid inclusions generally decrepitated at temperatures of about 300 °C prior to final homogenization. Unfortunately, the halite dissolution temperature was not measured.

4.3.3. Late stage

$T_{m\text{-}ice}$ of W-type aqueous inclusions from the late-stage quartz was observed between −0.3 °C and −2.3 °C (Table 1), corresponding to salinities varying from 0.35 to 3.87 wt.% NaCl equivalent. The homogenization occurs to the liquid phase between 120 °C and 214 °C.

4.4. Laser Raman spectroscopy

To constrain the composition of fluid inclusions, representative samples were examined using laser Raman microspectroscopy. Laser Raman spectroscopic analyses were performed at the Instrumental Analysis and Research Center, Sun Yet-sen University. Fluid inclusions were analyzed on a Renishaw RW-1000 Laser Raman microspectrometer. The laser source was an argon ion laser with a wavelength of 514.5 nm and a source power of 20 mW×100%. The spectral range falls between 50 and 4000 cm^{-1}. The data (Fig. 8) show that CO_2 and H_2O are the main volatiles in the measured fluid inclusions from the early-stage quartz, but some small quantities of CH_4 and N_2 are present in those from middle-stage quartz.

5. Discussion

5.1. Fluid boiling, mixing and gold mineralization

It has been suggested that fluid boiling is an important mechanism associated with ore–metal deposition in many hydrothermal deposits (Coulibaly et al., 2008; Fan et al., 2003; Yao et al., 2001).

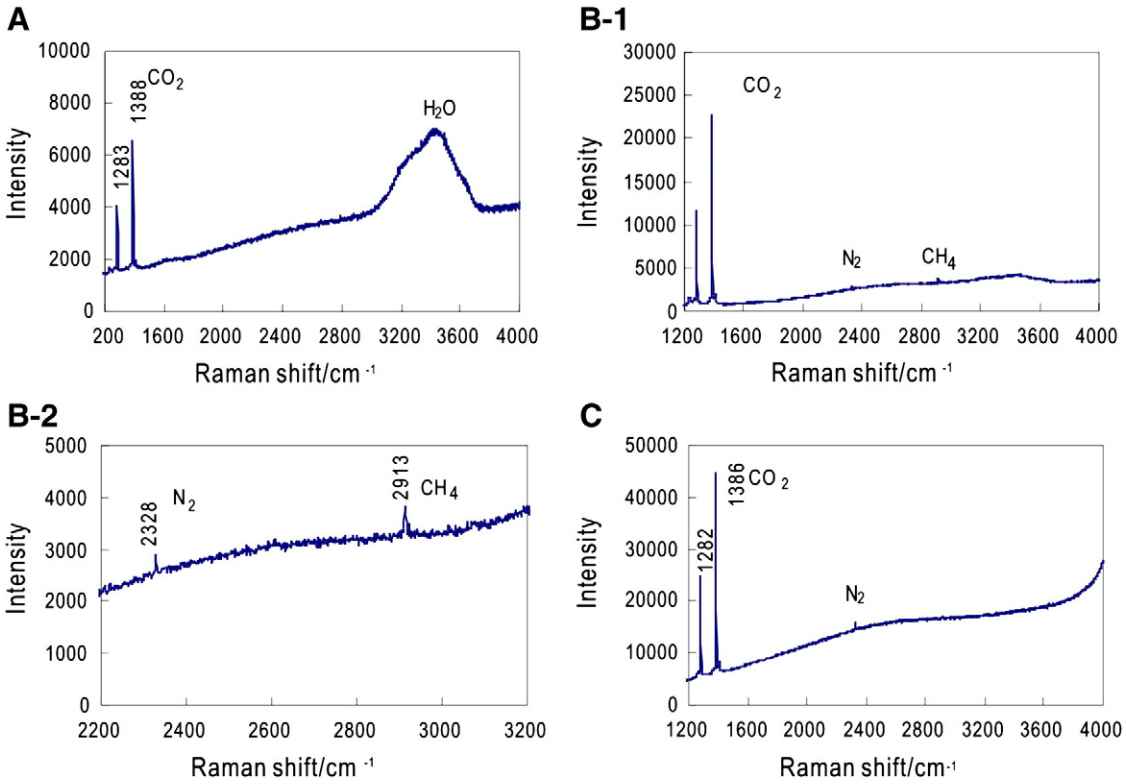

Fig. 8. Representative Raman spectra of vapor bubbles of fluid inclusions in quartz. Panel A shows that the vapor bubbles of early-stage CO_2–H_2O inclusions are mainly of CO_2; the other panels (B-1, B-2, and C) show that the bubbles in middle-stage fluid inclusions contain some CH_4 and N_2 in addition to CO_2.

Boiling of fluids at the Wangfeng gold deposit is strongly supported by petrographic observations showing that four different types of fluid inclusions coexist in the middle (mineralization)-stage quartz. Microthermometric analysis provides more evidence for fluid boiling: (1) the coexisting vapor- and liquid-rich fluid inclusions show a very similar range of homogenization temperatures and they have opposite modes of homogenization (V→L vs. L→V); and (2) variations of salinities of the fluids may also reflect fluid boiling (Roedder, 1984). In the middle-stage quartz, W-type fluid inclusions have salinities about 4.8 wt.% NaCl equivalent (average), accompanied by some S-type halite-bearing fluid inclusions, whereas coexisting C-type inclusions have average salinities less than 2.9 wt.% NaCl equivalent. The higher salinity of the liquid-rich W-type inclusions may be a direct result of boiling or effervescence of the CO_2–H_2O fluids during depressurization leading to a concentration of salts in the aqueous fluids and to the formation of halite-bearing inclusions (Roedder, 1984). Fluid boiling during mineralization and the resulted daughter-mineral-bearing fluid inclusions have been frequently reported in the orogenic lode deposits worldwide (Chen et al., 2004, 2012a; Deng et al., 2008; Hagemann and Luders, 2003; Qi et al., 2007; Zhang et al., 2004). Extensive fluid boiling may occur in the mineralization stage at Wangfeng. The boiling-resulted CO_2 escapes as indicated by fluid inclusion populations, associates with consumption of H^+ ($H^+ + HCO_3^- =$ $H_2O + CO_2$), and causes decomposing of $[Au(HS)_2]^-$ and precipitation of native gold, due to the activity of H^+ is the key factor to maintain HS^- and $[Au(HS)_2]^-$ stable in the fluids (Chen et al., 2007). Meanwhile, fluid immiscibility could release H_2S from liquid phase into vapor phase, which decreases the stability of Au–S complexes and subsequently precipitates Au from fluid (Cox et al., 1995; Jia et al., 2000; Naden and Shepherd, 1989).

Although fluid boiling is crucial during mineralization stage, some fluid characteristics, such as decreasing of homogenization temperature in the same sample, variation of salinities and complicated vapor components (CO_2, CH_4 and N_2), cannot be solely explained by fluid boiling and may also indicate that fluid mixing occurred in the middle mineralization stage, e.g., with low-temperature and low-salinity meteoric water which is supported by H–O stable isotopes (Chen et al., 2000). Fluid mixing, or inflow of the meteoric fluids, will effectively destabilize the $[Au(HS)_2]^-$ ligand resulting in the precipitation of native gold and pyrite, according to the reaction: $2HCO_3^- + [Au(HS)_2]^- + Fe^{3+} =$ $Au + FeS_2 + 2H_2O + 2CO_2$. Fluid mixing has been documented in many orogenic-type gold deposits, including the Sawayaerdun gold deposit in the Chinese Southern Tian Shan (Bierlein and Maher, 2001; Brown, 1998; Chen et al., 2004; Chen et al., 2012a).

5.2. Pressure and depth of gold deposition

Most C-type fluid inclusions in early- and middle-stage quartz from the Wangfeng gold deposit have $T_{m\text{-}CO_2}$ values below or near −56.6 °C, which are interpreted as indicating the presence of other species such as CH_4 or N_2. The presence of CH_4 and/or N_2 in the CO_2–H_2O–NaCl system may affect some microthermometric properties and can cause misestimates of fluid salinity, density, and trapping pressure (Van den Kerkhof and Thiéry, 2001) (Table 2). However, the consistency of the salinity data precludes a significant influence of the CH_4 and N_2 contents, except for a few $T_{m\text{-}clath}$ values greater than 10 °C that are likely related to the presence of appreciable amounts of CH_4 or N_2. Therefore,

Table 2
Density and trapping pressure of fluid inclusions of the Wangfeng gold deposit.

Metallogenic stage	Type	$T_{h,tot}$ (°C)	X_{CO_2}	CO_2 density (g/cm^3)	Bulk density (g/cm^3)	Trapping pressure (MPa)
Early stage	C	270–360	0.3–0.9	0.56–0.87	0.73–0.89	110–300
Middle stage	C	210–340	0.1–0.7	0.71–0.9	0.77–0.95	90–250

X_{CO_2} = mole fraction of CO_2 in the vapor phase.

the salinities determined from the largely predominant group of fluid inclusions are considered as good estimates of the fluid composition. Using the Flincor program of Brown (1989) and the equations of Brown and Lamb (1989) for the CO_2–H_2O–NaCl system, the calculated pressure was 110–330 MPa in the early stage and 90–250 MPa in the middle stage, respectively. The trapping pressure in the early stage should be higher than 110–330 MPa considering the effects of depth, whereas that of the middle stage is equal to 90–250 MPa given fluid boiling occurring at this stage. Given 1.0 g/cm^3 as a density of fluid and 2.7 g/cm^3 as an average density of rock, the Wangfeng gold deposit is estimated to have been formed at paleodepths of approximately 9 to over 11 km, which documents an uplift of more than 2 km for the orebody from the early stage. As a result, the Wangfeng gold deposit corresponds to hypozonal regimes of orogenic gold deposits proposed in the literature (typically 5–18 km; Chen, 2006; Groves et al., 1998). The wide range of pressures is a common phenomenon in orogenic deposits and could have been promoted by the seismic activity related to uplift and exhumation in orogenic environments (Deng et al., 2008; Qi et al., 2007; Sibson, 1987). Depressurization during uplift could trigger the precipitation of quartz and metals and also fluid boiling discussed above.

5.3. Fluid evolution in the Wangfeng gold deposit

In the Late Carboniferous and Permian, microcontinent collision occurred between the Tarim–Kazakhstan and Siberia plates as a consequence of the Andean-type subduction and closure of the western section of the Paleotethys Ocean, which generated extensive compression, crustal shortening, thickening and uplift in the Tian Shan area (Fig. 1; Charvet et al., 2011; Xiao et al., 2008). During this stage, the Hongwuyueqiao Fault acted as a southward intracontinental subduction zone. The Carboniferous Qiergusitao Group, which is composed of thick-bedded clastic rocks, andesitic lava, and breccia intercalated with limestone, chert and shale, was subducted down the Hongwuyueqiao Fault to the Wangfeng ore field, reworked, and metamorphosed by increasing temperature and pressure (Fig. 9A; Chen et al., 2000). Decarbonization of carbonate in the subducted sediments (generally over 300 °C) could have produced $^{13}\delta$C-rich CO_2 fluids (Chen et al., 2000), which is consistent with microthermometric data obtained in the early-stage quartz, i.e., the molar percentage of CO_2 in the fluids in the early stage is between 30% and 90%, with densities of 0.89 to 0.73 g/cm^3 and salinities of 1.62 to 8.03 wt.% NaCl equivalent, and homogenization temperatures between 260 °C and 390 °C (Table 1). With continuous crustal uplift and erosion, the deeply-buried early quartz veins and structural zones were uplifted resulting in decompression. This change in tectonic conditions led to the fluids trapped in structural zones to experience extensive fluid immiscibility due to decreasing pressure (Cox et al., 1995; Chen et al., 2012b) and precipitated quartz and also Au and pyrite at medium temperatures (210–340 °C; Fig. 9B). Fluid mixing, which could have been dominated by meteoric water modified by rock–fluid reactions, may have also occurred during the mineralization stage generating complicated fluid compositions, e.g., complicated fluid inclusion types and presence of CH_4 and N_2 in fluid inclusions from the middle-stage quartz. Following the main mineralization stage at Wangfeng, the regional heat source and associated hydrothermal fluid circulation dissipated, accompanied by a drop of temperatures (<220 °C). During the final stage, local and usually barren, carbonate (–quartz) veinlets formed (Fig. 9C). However, the continuing subduction and increasing temperature (to approximately 700 °C) could have partially melted the rocks to produce S-type granitic magmas, e.g., the Wulasitai granite in the south of Wangfeng (Fig. 9).

5.4. Orogenic-type model for the Wangfeng gold deposit

Orogenic gold deposits represent a coherent group of widely distributed deposits in accretionary or collisional orogens of all ages. They form

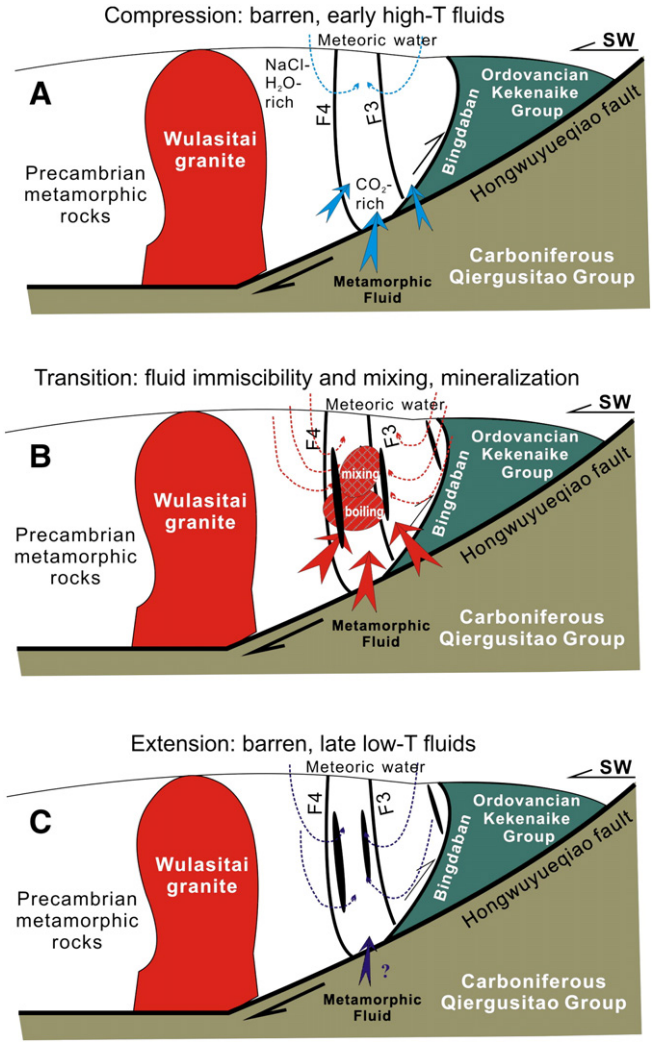

Fig. 9. Fluid evolution model of the Wangfeng gold deposit: A) Early stage high-temperature metamorphic fluids formed CO_2-rich fluids in trapping areas during compression. B) Middle stage mineralization was formed through fluid immiscibility and mixing during the compression–extension transitional stage. C) Late stage low-temperature barren fluids form carbonate–quartz veins during extension.

over an extended depth range from 5 to 20 km (Kerrich, 1999), although most commonly in greenschist-facies host rock and from a relatively uniform, deep source. In many terranes, first-order crustal-scale faults and shear zones control the regional distribution of the deposits. Orogenic gold deposits, as exemplified by the gold deposits of the Yilgarn Block, Western Australia, and the Ashanti Au deposit, Ghana, are predominantly vein-hosted, low sulfide, and epigenetic and generally have low salinity (5 to 8 wt.% NaCl equivalent; Chen, 2006; Groves et al., 1998). The orebodies in the Wangfeng gold deposit formed in a typical orogenic setting and are located in ductile shears and faults, with mineralization styles dominated by auriferous quartz veins and disseminated ores. The hydrothermal alteration consists of silicification, sericitization, chloritization, carbonation, and sulfidation. The sulfide content of the auriferous veins is of low sulfide volume, commonly less than 3%. Orogenic ore-forming hydrothermal systems are dominated by low-salinity and CO_2-rich fluids with relatively heavy oxygen isotope values of hydrothermal quartz (Chen et al., 1998; Chen et al., 2000). There is no direct space relationship with intrusions (e.g., the Wulasitai granite) and stable isotopes of ore-forming fluids also preclude apparent genetic relationships with igneous rocks although such connection cannot be entirely excluded (Chen et al., 2000). Furthermore, the

mineralization and alteration characteristics of the Wangfeng deposit are also distinct from other documented epithermal and intrusion-related gold deposits (Hedenquist et al., 2000; Thompson et al., 1999). All of these features are in agreement with the orogenic gold deposit. As a result, we suggest that the Wangfeng gold deposit is an orogenic-type deposit.

6. Conclusions

(1) In the Wangfeng gold deposit, there are four types of fluid inclusions present in quartz, including: CO_2–H_2O (C type), pure CO_2 (PC type), NaCl–H_2O (W type), and daughter-mineral-bearing (S type). Quartz that formed in the early and middle stages contains abundant C-type fluid inclusions, but in the late-stage quartz only W-type fluid inclusions are present. S-type fluid inclusions were only identified in the middle (mineralization) stage.

(2) The mineralizing fluids were initially low salinity, mesothermal, CO_2-rich and originated from metamorphic fluids. These fluids evolved to lower temperature, CO_2-poor, and meteoric water-dominated fluids in the late stage. Gold deposition is possibly a consequence of boiling of an original H_2O–CO_2 fluid in response to pressure and temperature fluctuations.

(3) The Wangfeng gold deposit belongs to a hypozonal orogenic gold deposit formed in an intercontinental-collision tectonic setting during the Late Carboniferous and Permian.

Acknowledgments

This study was financed jointly by the National Basic Research Program 973 Project 2007CB411303, the National Science and Technology Infrastructure Program 2007BAB25B03, and NSFC nos. 41072062 and 40730421. We sincerely thank members of the Office of Project 305, Professor Li Chaoyang, Professor Wu Guang, Dr. Zhongwei, and the staff of the Wangfeng Gold Mine, who offered help with sampling in the field. We also thank Drs. Li Jing and Zhu Mingtian for their laboratory help. Suggestions from the Editor, Franco Pirajno, and two anonymous reviewers have remarkably improved the quality of this paper.

References

Bierlein, F.P., Maher, S., 2001. Orogenic disseminated gold in Phanerozoic fold belts — examples from Victoria, Australia and elsewhere. Ore Geol. Rev. 18, 113–148.
Bodnar, R.J., 1993. Revised equation and table for determining the freezing point depression of H_2O–NaCl solutions. Geochim. Cosmochim. Acta 57, 683–684.
Brown, P.E., 1989. Flincor: a microcomputer program for the reduction and investigation of fluid inclusion data. Am. Mineral. 74, 1390–1393.
Brown, P.E., 1998. Fluid inclusion modeling for hydrothermal systems. Rev. Econ. Geol. 10, 151–171.
Brown, P.E., Lamb, W.M., 1989. P–V–T properties of fluids in the system $H_2O \pm CO_2 \pm$ NaCl: new graphic presentations and implications for fluid inclusion studies. Geochim. Cosmochim. Acta 53, 1209–1221.
Charvet, J., Shu, L.S., Laurent-Charvet, S., Wang, B., Faure, M., Cluzel, D., Chen, Y., Jong, K.D., 2011. Palaeozoic tectonic evolution of the Tianshan belt, NW China. Sci. China D 54, 166–184.
Chen, Y.J., 2000. Progress in the study of Central Asia-type orogenesis — metallogenesis in northwest China. Geol. J. China Univ. 6, 17–22 (in Chinese with English abstract).
Chen, Y.J., 2006. Orogenic-type deposits and their metallogenic model and exploration potential. Geol. China 33, 1181–1196 (in Chinese with English abstract).
Chen, Y.J., 2010. On epizonogenism and genetic classification of hydrothermal deposits. Earth Sci. Front. 17, 27–34 (in Chinese with English abstract).
Chen, Y.J., Fu, S.G., 1992. Gold Mineralization in West Henan, China. Seismological Press, Beijing, p. 234 (in Chinese with English abstract).
Chen, B., Jahn, B.M., 2004. Genesis of post-collisional granitoids and basement nature of the Junggar Terrane, NW China: Nd–Sr isotope and trace element evidence. J. Asian Earth Sci. 23, 691–703.
Chen, Y.J., Li, X., Jing, J., Gao, X.L., Chen, H.Y., Wu, X.D., Wu, D.H., 1998. Study of ore-forming fluid for the Wangfeng gold deposit of Xinjiang and its genetic implication. Bull. Chin. Acad. Geol. Sci. 19, 195–203 (in Chinese with English abstract).
Chen, H.Y., Bao, J.X., Zhang, Z.J., Liu, Y.L., Ni, P., Ling, H.F., 2000. Isotope indication to source of ore materials and fluids of the Wangfeng gold deposit in Tianshan: a case study of metallogenesis during collisional orogenesis. Sci. China D 43, 156–166.
Chen, Y.J., Chang, X.L., 2000. Copper and Gold Metallogeny and Exploration Targeting in the Tiange'er–Baluntai Region. Beijing: Report 96-915-03-05A of the National Research Project, 305, pp. 1–54 (in Chinese).
Chen, Y.J., Pirajno, F., Sui, Y.H., 2004. Isotope geochemistry of the Tieluping silver deposit, Henan, China: a case study of orogenic silver deposits and related tectonic setting. Miner. Deposita 39, 560–575.
Chen, Y.J., Ni, P., Fan, H.R., Pirajno, F., Lai, Y., Su, W.C., Zhang, H., 2007. Diagnostic fluid inclusions of different types hydrothermal gold deposits. Acta Petrol. Sin. 23, 2085–2108 (in Chinese with English abstract).
Chen, Y.J., Zhai, M.G., Jiang, S.Y., 2009. Significant achievement and open issue in study of orogenic and metallogenesis surrounding the North China continent. Acta Petrol. Sin. 25, 2695–2726 (in Chinese with English abstract).
Chen, Y.J., Pirajno, F., Wu, G., Qi, J.P., Xiong, X.L., Zhang, L., 2012a. Epithermal deposits in north Xinjiang, NW China. Int. J. Earth Sci. 101, 889–917.
Chen, H.Y., Chen, Y.J., Baker, M., 2012b. Evolution of ore-forming fluids in the Sawayaerdun gold deposit — the first Muruntau-like gold deposit in the Southwestern Chinese Tianshan metallogenic belt. J. Asian Earth Sci. 49, 131–144.
Collins, P.L.F., 1979. Gas hydrates in CO_2-bearing fluid inclusions and use freezing data for estimation of salinity. Econ. Geol. 74, 1435–1444.
Coulibaly, Y., Boiron, M.C., Cathelineau, M., Kouamelan, A.N., 2008. Fluid immiscibility and gold deposition in the Birimian quartz veins of the Angovia deposit (Yaoure, Ivory Coast). J. Afr. Earth Sci. 50, 234–254.
Cox, S.F., Sun, S.S., Etheridge, M.A., Wall, V.J., Potter, T.F., 1995. Structural and geochemical controls on the development of turbidite-hosted gold quartz vein deposits, Wattle Cully mine, central Victoria, Australia. Econ. Geol. 90, 1722–1746.
Deng, X.H., Li, W.B., Li, N., Mei, M., Zhang, Y., 2008. Study of fluid inclusions and genesis of the Zhifang Mo deposit in Songxian County, Henan Province. Acta Petrol. Sin. 24, 2133–2148 (in Chinese with English abstract).
Fan, H.R., Xie, Y.H., Zhai, M.G., Jin, C.W., 2003. A three stage fluid flow model for Xiaoqinling lode gold metallogenesis in the Henan and Shaanxi provinces, central China. Acta Petrol. Sin. 19, 260–266 (in Chinese with English abstract).
Geological Team 1 of the Xinjiang Bereau of Geology and Mineral Resources, 2005. The prospecting report for No.12 orebody of the Wangfeng deposit, xinjiang, p. 42.
Goldfarb, R.J., Snee, L.W., Miller, L.D., Newberry, R.J., 1991. Rapid dewatering of the crust deduced from ages of mesothermal gold deposits. Nature 354, 296–298.
Goldfarb, R.J., Groves, D.I., Gardoll, S., 2001. Orogenic gold and geologic time: a global synthesis. Ore Geol. Rev. 18, 1–75.
Groves, D.I., Beirlein, F.P., 2007. Geodynamic settings of mineral deposit systems. J. Geol. Soc. 164, 19–30.
Groves, D.I., Goldfarb, R.J., Gebre-Mariam, M., Hagemann, S.G., Robert, F., 1998. Orogenic gold deposits: a proposed classification in the context of their crustal distribution and relationship to other gold deposit types. Ore Geol. Rev. 13, 7–27.
Hagemann, S.G., Luders, V., 2003. P–T–X conditions of hydrothermal fluids and precipitation mechanism of stibnite–gold mineralization at the Wiluna lode–gold deposits, Western Australia: conventional and infrared microthermometric constraints. Miner. Deposita 38, 936–952.
Hedenquist, J.W., Arribas Jr., A., Gonzales-Urien, E., 2000. Exploration for epithermal gold deposits. Rev. Econ. Geol. 13, 245–277.
Jia, Y., Li, X., Kerrich, R., 2000. A fluid inclusion study of Au-bearing quartz vein systems in the central and north Deborah deposits of the Bendigo gold field, central Victoria, Australia. Econ. Geol. 95, 467–495.
Kerrich, R., 1999. Nature's gold factory. Science 284, 2101–2102.
Kerrich, R., Goldfarb, R.J., Groves, D.I., Garwin, S., Jia, Y.F., 2000. The characteristics, origins and geodynamic settings of supergiant gold metallogenic provinces. Sci. China D 43, 1–68.
Naden, J., Shepherd, T.J., 1989. Role of methane and carbon dioxide in gold depositions. Nature 342, 793–795.
Pirajno, F., 2009. Hydrothermal Processes and Mineral Systems. Springer, Perth, p. 1250.
Qi, J.P., Chen, Y.J., Ni, P., Lai, Y., Ding, Y.J., Song, Y.W., Tang, G.J., 2007. Fluid inclusion constraints on the origin of the Lengshuibeigou Pb–Zn–Ag deposit, Henan Province. Acta Petrol. Sin. 23, 2119–2130 (in Chinese with English abstract).
Roedder, E., 1984. Fluid inclusions. Rev. Mineral. 12, 1–644.
Sengor, A.M.C., Natal'in, B.A., 1996. Paleotectonics of Asia: fragments of synthesis. In: Yin, A., Harrison, T.M. (Eds.), The Tectonic Evolution of Asia. Cambridge University Press, Cambridge, pp. 480–640.
Sibson, R.H., 1987. Earthquake rupturing as a mineralizing agent in hydrothermal systems. Geology 15, 701–704.
Thompson, J.F.H., Sillitoe, R.H., Baker, T., Lang, J.R., Mortensen, J.K., 1999. Intrusion-related gold deposits associated with tungsten–tin provinces. Miner. Deposita 34, 323–334.
Van den Kerkhof, A.M., Thiéry, R., 2001. Carbonic inclusions. Special volume in honour of Jacques Touret. Fluid inclusions: phase relationships–methods–applications. In: Andersen, T., Frezzotti, M.L., Burke, E.A.J. (Eds.), Lithos, 55, pp. 49–68.
Wang, J.L., Liu, Y.J., Wang, R.S., 1994. Ductile shear zone and the relationship with gold deposits in Shenglidaban gold field, Xinjiang. Northwest Geosci. 15, 20–26 (in Chinese with English abstract).
Wang, J.L., Liu, Y.J., Wang, R.S., 1995. Auriferous mineralization of the Shenlidaban gold field, Xinjiang. J. Northwest Univ. (Nat. Sci. Ed.) 25, 142–146 (in Chinese with English abstract).
Wu, X.D., Chen, G.J., 1999. Geological characteristics and metallogenetic regulation of Wangfeng gold mineralization zone in west part of Tianshan Mountains. Xinjiang Geol. 17, 20–26 (in Chinese with English abstract).
Xiao, W.J., Han, C.M., Yuan, C., Sun, M., Lin, S.F., Chen, H.L., Li, Z.L., Li, J.L., Sun, S., 2008. Middle Cambrian to Permian subduction-related accretionary orogenesis of northern Xinjiang, NW China: implications for the tectonic evolution of Central Asia. J. Asian Earth Sci. 32, 102–117.

Xiao, W.J., Windley, B.F., Huang, B.C., Han, C.M., Yuan, C., Chen, H.L., Sun, M., Sun, S., Li, J.L., 2009. End-Permian to mid-Triassic termination of the southern Altaids: implications for the geodynamic evolution, Phanerozoic continental growth, and metallogeny of Altay Asia. Int. J. Earth Sci. 98, 1189–1217.

Yao, Y., Murphy, P.J., Robb, L.J., 2001. Fluid characteristics of granitoid-hosted gold deposit in the Birrimian Terrane of Ghana: a fluid inclusion microthermometric and Raman spectroscopic study. Econ. Geol. 96, 1611–1643.

Zhang, J., Chen, Y.J., Li, G.P., Li, Z.L., Wang, Z.G., 2004. Characteristics of ore geology and fluid inclusion of the Yindonggou silver deposit, Neixiang County, Henan Province: implication for metallogenic type. J. Mineral. Petrol. 24, 55–64 (in Chinese with English abstract).

Zhu, Y.F., Zhou, J., Zeng, Y.S., 2007. The Tianger (Bingdaban) shear zone hosted gold deposit, west Tianshan, NW China: petrographic and geochemical characteristics. Ore Geol. Rev. 32, 337–365.